

Multilamellar Vesicle Formation from a Planar Lamellar Phase under Shear Flow

Luigi Gentile,*^{†,‡} Manja A. Behrens,[‡] Lionel Porcar,[§] Paul Butler,^{||} Norman J. Wagner,^{||,⊥} and Ulf Olsson[‡]

[†]Department of Chemistry and Chemical Technologies, University of Calabria, Pietro Bucci 12C, 87036 Rende, Italy

[‡]Division of Physical Chemistry, Lund University, P.O. Box 124, SE-221 00 Lund, Sweden

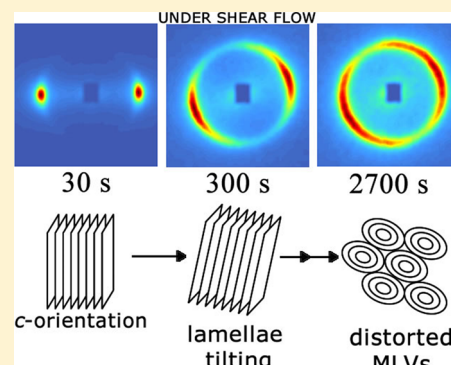
[§]Large Scale Structure Group, Institut Laue Langevin, Grenoble, France

^{||}NIST Center for Neutron Research (NCNR), Gaithersburg, Maryland 20899, United States

[⊥]Center for Neutron Science, Department of Chemical and Biomolecular Engineering, University of Delaware, 150 Academy Street, Newark, Delaware 19716, United States

Supporting Information

ABSTRACT: The formation of multilamellar vesicles (MLVs) from the lamellar phase of nonionic surfactant system $C_{12}E_5/D_2O$ under shear flow is studied by time-resolved small angle neutron and light scattering during shear flow. A novel small angle neutron scattering sample environment enables the tracking of the lamellae alignment in the velocity–velocity gradient (1–2) plane during MLV formation, which was tracked independently using flow small angle light scattering commensurate with rheology. During the lamellar-to-multilamellar vesicle transition, the primary Bragg peak from the lamellar ordering was observed to tilt, and this gradually increased with time, leading to an anisotropic pattern with a primary axis oriented at $\sim 25^\circ$ relative to the flow direction. This distorted pattern persists under flow after MLV formation. A critical strain and critical capillary number based on the MLV viscosity are demonstrated for MLV formation, which is shown to be robust for other systems as well. These novel measurements provide fundamentally new information about the flow orientation of lamellae in the plane of flow that cannot be anticipated from the large body of previous literature showing nearly isotropic orientation in the 2,3 and 1,3 planes of flow. These observations are consistent with models for buckling-induced MLV formation but suggest that the instability is three-dimensional, thereby identifying the mechanism of MLV formation in simple shear flow.



1. INTRODUCTION

In an ideal lamellar phase (L_α), surfactants are organized in essentially flat and infinite bilayers, which are stacked with one-dimensional order with a thickness of the water layer on the order of nanometers.^{1,2} In many systems, these layered structures are found to be unstable under shear flow and the structure transforms to multilamellar vesicles (MLVs), also called “onions”.^{3–34} However, in these lamellar systems the lamellae can align in the flow field with their layer normal along the velocity gradient, c orientation, or in the vorticity direction, a orientation;^{35,36} at low shear rate the c orientation is most prevalent, while at higher shear rate the a orientation is prevalent.^{7,25}

Roux and coworkers first observed the L_α -to-MLV transition in a sodium dodecyl sulfate/pentanol/water/decane system.⁶ The critical shear rate for the transition to MLVs was found to be proportional to the cube of the membrane volume fraction. Additionally, they showed that increasing the shear rate induces a transformation from the MLV state to oriented lamellae.⁷ Moreover, the radius of MLVs, R , follows approximately

$$R \propto \dot{\gamma}^{-1/2} \quad (1)$$

$$R \propto d^{-2} \propto \phi^2 \quad (2)$$

where $\dot{\gamma}$ is the shear rate, d is the lamellar spacing, and ϕ is the membrane volume fraction. Note that MLV formation has been shown to be controlled by stress rather than shear rate in some systems, highlighting the direct connection between the stresses acting across an MLV by the applied deformation and MLV size,³⁷ in which case $R \propto \sigma^{-1/2}$ for elastic bending,⁶ with σ being the shear stress. An alternative theory by van der Linden and Droege predicts $R \propto \sigma^{-1}$, which follows from the classical capillary number of fluid mechanics whereby viscous forces balance interfacial tension.^{37,38}

The saddle-splay modulus is important for the stability of the bilayer structures mainly with respect to temperature,⁸ while the bending modulus is related to structural parameters, i.e., to the molecular structure, of the bilayer and describes how much energy is required to bend a surfactant film.⁹ Nonionic ethylene oxide (E) surfactant water systems are known to be susceptible

Received: April 16, 2014

Revised: June 28, 2014

Published: July 1, 2014

to shear flow, especially the lamellar phase due to the low bending rigidity.⁹ For this reason, the aqueous nonionic surfactant systems of the C_nE_m type ($C_nH_{2n+1}(OC_2H_4)_mOH$)^{8–22,28} are observed to undergo shear-induced transitions.

The structural evolution from lamellae to MLVs has been followed by time-resolved viscosity measurements,^{6,9–12,23–25,37} small angle light scattering (SALS),^{6–9,12,18,23,37,39} small angle neutron scattering (SANS),^{7–13,16,18–20,25} and small angle X-ray scattering (SAXS).^{16,17,22,40} Experimentally, the MLV formation is associated with a four-lobe cloverleaf pattern in the depolarized SALS data.

The pathway of the MLV formation under shear flow has been characterized by an intermediate structure between the planar lamellae and the MLVs identified as multilamellar cylinders (MLCs).^{12,28,29} The SALS pattern at this stage displays an elongated pattern perpendicular to the flow direction, and one also often observes a plateau in the viscosity profile. The anisotropic self-diffusion of water in this intermediate state confirms the cylindrical symmetry.^{15,28} After the transition stage, the viscosity continues to increase and the two-lobe SALS pattern evolves into a four-lobe pattern.

Theoretical approaches to explain the L_α -to-MLV transition have been reported by several authors. Roux et al.⁶ derived eq 1 by balancing the viscous and elastic stresses. This approach, however, could not predict eq 2. An alternative approach was proposed by van der Linden,²³ who derived a theoretical expression balancing the surface stress with the shear stress $R \propto \phi^{2\gamma^{-1/2}}$. However, neither of these approaches propose a mechanism for formation. Such a mechanism was suggested by Zilman and Granek,⁴¹ who proposed that the formation of MLVs occurs due to the coupling of short-wavelength thermal undulations with strain, which leads to a coherent stripe buckling of the lamellae that eventually results in an instability leading to MLV formation. In this model, MLVs are formed via the coherent buckling of lamellae above a critical shear rate $\dot{\gamma}_C \propto d^{-5/2}D^{-1/2} \propto \phi^{5/2}D^{-1/2}$, where D is the gap spacing. This result was experimentally confirmed by Courbin et al.^{42,43} Marlow and Olmsted⁴⁴ considered the suppression of the undulations in shear flow by modeling the flow as an effective anisotropic tension, which decreases the compression modulus. When new layers can be generated by permeation or defects, then a decrease in lamellar spacing occurs. On the other hand, when the system cannot change the number of layers or the process is very slow, an instability is induced for tension larger than $\sigma_C \propto (dD)^{-1}$, and this instability produces either multilamellar cylinders or vesicles. Marlow and Olmsted predict the critical shear rate $\dot{\gamma}_C \propto d^{-2}D^{-1} \propto \phi^2D^{-1}$, where the exponents are slightly different from what was obtained by Zilman and Granek. In both cases, the absolute value of the critical shear rate obtained experimentally is much smaller than predicted by theory; however, Zilman and Granek⁴¹ and qualitatively Diat et al.⁷ resolved this discrepancy by renormalizing by the solution viscosity, which, due to defects, is typically orders of magnitude higher than predicted for a pure lamellar phase. As the viscosity of the solution varies substantially during MLV formation, the stresses acting on the MLV microstructure are tightly coupled to the structure being formed such that the shear stress is the relevant measure rather than the ideal lamellar viscosity times the shear rate.³⁷

Although several authors for a large variety of surfactant systems already document the L_α -to-MLV transition under shear flow, the actual mechanism by which MLVs form under shear flow is not proven. In particular, the experiments to date

view MLV formation in the velocity–vorticity (1–3) and/or velocity gradient–vorticity (2–3) plane(s) of flow and thus miss the important observation of the possible buckling of the lamellar phase in the velocity–velocity gradient plane. Indeed, Zilman and Granek propose a highly anisotropic buckled lamellar phase under shear flow as the instability leading to MLV formation.

The experiments reported here are performed on the $C_{12}E_5/D_2O$ system for which at 40 wt % surfactant MLV formation was reported at 55 °C.¹⁰ In this previous study, rheo-nuclear magnetic resonance and rheo-SANS in the velocity–vorticity plane were used to report the L_α -to-MLV transition. Here, the structural transition between L_α and MLVs was followed by time-resolved small angle neutron scattering in the velocity–shear gradient (1–2) plane.^{45,46} This new point of view offers interesting insight into the mechanism by which the planar lamellae buckle and fold to form multilamellar vesicles and is shown to be essential to testing theories for MLV formation. The experiments were performed for 40 wt % surfactant over the entire temperature region where the lamellar phase exists, i.e., between 55 and 70 °C, at shear rates of between 10 and 200 s⁻¹. Complementary rheo-small angle light scattering experiments were performed in the shear rate range between 10 and 200 s⁻¹ to obtain the MLV sizes. Combining the information from 1–2 plane flow-SANS and the rheo-SALS experiments provides new insight into the transition mechanism.

2. EXPERIMENTAL SECTION

2.1. Materials. Pentaethylene glycol monododecyl ether ($C_{12}E_5$) was purchased from Nikko Chemicals Co., Ltd. (Tokyo, Japan). Deuterium oxide (D_2O) was purchased from Armar Chemicals. The purity of both materials was higher than 99.8%, and the materials were used without further purification. The sample was prepared by mixing the surfactant and D_2O in the desired weight fractions. The $C_{12}E_5$ water system at a concentration of 40 wt % shows a hexagonal (H_1) phase between 0 and 20 °C, a micellar solution (L_1) between 20 and 55 °C, and a lamellar phase (L_α) between 55 and 70 °C.⁴⁷ The experiments were performed in the lamellar phase state. Triethylene glycol monodecyl ether ($C_{10}E_3$) was also purchased from Nikko Chemicals Co., Ltd., and the $C_{10}E_3/D_2O$ system was prepared by mixing the surfactant and D_2O . The sample at 40 wt % was studied by flow-SANS.

2.2. Flow-SANS. Small angle neutron scattering (SANS) experiments were performed using the D22 instrument at the Institut Laue-Langevin (ILL), Grenoble, France.⁴⁸ A novel sample environment, 1–2 flow STR-SANS (spatiotemporally resolved small angle neutron scattering), is used to measure the surfactant microstructure on length scales from the atomic to that of the self-assembled lamellar microstructure.⁴⁵ In this environment, the sample is contained in an aluminum Couette with a radius of the inner cylinder of 25 mm, a gap of 1 mm, and a path length of 5 mm. The neutron beam traversed the shear cell through the gap, i.e., the scattering is observed in the 1–2 plane expanded by the flow and the shear gradient directions (Supporting Information).⁴⁶ A slit preceding the cell reduced the neutron beam to 0.5 mm in width by 3.0 mm in height.

The neutron wavelength was 6 Å, and the sample-to-detector distance was 3 m, covering a q range of 0.019–0.24 Å⁻¹. Raw SANS data were reduced in GRASansP v.6.79, correcting the two-dimensional scattering patterns by the detector efficiency map. The scattering data were normalized by the incident beam flux on the sample and by the sample thickness to obtain the intensity scale (scattering cross section per unit volume). After sample loading, SANS experiments were performed without applying a controlled shear flow. The patterns were recorded (i) immediately after loading, (ii) during shear flow experiments, and (iii) after the system reaches equilibrium.

The measurements were performed in a wide range of temperatures. In the flow-SANS experiments, evaporation was avoided by using a sealed Couette. The temperature of the sample was controlled to within ± 0.5 °C by an external thermostatic water bath. The system was loaded in the Couette cell using a syringe and heated from 45 to 55 °C by applying a shear rate of 1 s⁻¹, resulting in an aligned lamellar state at 55 °C. The heating process from 45 to 55 °C required 10 min. The acquisition time was 30 s for each 2D pattern except for the start–stop experiments in Figure 5, where it was reduced at 15 s.

The same 1–2 flow Couette SANS sample environment was used to study the C₁₀E₃/D₂O system at the NG3 30 m SANS instrument at the NIST Center for Neutron Research.⁴⁹ Acquisition times were 60 s. Here, the slit used was a semicircular shape with 0.8 mm width, resulting in slight shadowing effects from the outer and inner cylinders. This can in principle be corrected for, but here we used only the peak position which is unaffected by the shadowing.

2.3. Rho-SALS. Small angle light scattering (SALS) experiments were performed in the velocity–vorticity (1–3) plane using an Anton Paar Physica MCR 301 equipped with quartz cone–plate geometry (0.188 mm gap). In all measurements, a 10 mW diode laser operating at a wavelength of 658 nm was used as the light source. Depolarized (polarizer and analyzer perpendicular) SALS patterns were captured using a CCD camera (Lumenera Corporation, Ottawa, Canada) located below the screen on which the scattered light was directed. The incoming beam traveled along the velocity gradient direction, and the scattering pattern was detected in the velocity–vorticity plane. The experiments were performed at 55 °C by applying shear rates of 10 and 60 s⁻¹.

3. RESULTS AND DISCUSSION

3.1. MLV Formation by Rho-SALS. The temporal development of MLVs and their size in the shear rate range between 10 and 200 s⁻¹ at 55 °C (Figure 1) were obtained using rheo-SALS experiments in the 1–3 plane of flow. Starting with the lowest shear rate of 10 s⁻¹, the samples show no discernible scattering other than noise about the beamstop, which is characteristic for an L_a phase in the c orientation, until

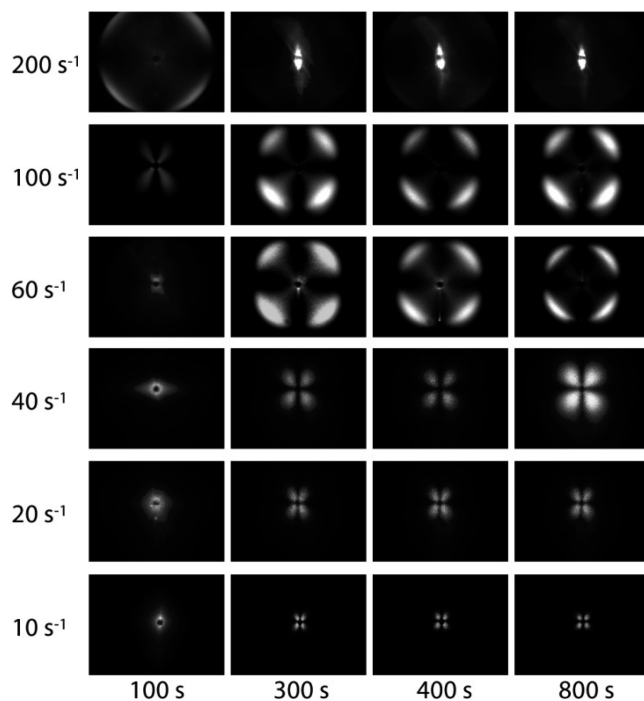


Figure 1. SALS patterns obtained at 55 °C for the C₁₂E₅/D₂O system at shear rates of between 10 and 200 s⁻¹.

around 300 s, when a characteristic four-lobe pattern appears that is due to MLVs.⁵⁰ Increasing the shear rate leads to an increase in the scattering, which indicates a reduction in the size of the MLVs. As MLV formation is strain-dependent,³⁷ the characteristic MLV structure factor becomes evident by 300 s for higher shear rates. However, at 200 s⁻¹ the MLVs are not stable and the inverse transition between MLV and an L_a phase with the a orientation is observed after 300 s. These general features are in agreement with a previous study,¹⁰ where for shear rates beyond 10 s⁻¹ the C₁₂E₅ vesicles are not stable under steady shear flow. In the experiments reported here, a lower total strain is applied in order to characterize the MLV state. It should be noted that SALS patterns recorded in the velocity–vorticity plane are nearly symmetric and thus are not significantly distorted by the shear flow.

The characteristic vesicle radius (R_{MLV}) can be quantified from SALS patterns by fitting to the model proposed by Samuels:⁵⁰ for optically anisotropic spheres, $R_{\text{MLV}} = 4.1/q$, while for closely packed spheres, $R_{\text{MLV}} = 3.9/q$. The radii as a function of the applied shear rates are reported in Table 1,

Table 1. Shear Rate, Viscosity, MLV Radius, and Capillary Numbers^a

shear rate (s ⁻¹)	viscosity (Pa s)	MLV radius (μm)	Ca	Ca*
10	5.5 ± 0.3	4.1 ± 0.3	4.9 × 10 ⁻⁴	4.5 ± 0.6
20	4.5 ± 0.3	3.0 ± 0.3	7.2 × 10 ⁻⁴	5.4 ± 0.6
40	3.9 ± 0.2	1.9 ± 0.2	9.1 × 10 ⁻⁴	5.9 ± 0.4
60	1.9 ± 0.1	1.3 ± 0.2	9.4 × 10 ⁻⁴	3.0 ± 0.3
100	1.5 ± 0.1	1.0 ± 0.2	1.2 × 10 ⁻³	3.0 ± 0.3

^aViscosity values were measured using the Anton Paar Physica MCR 301 equipped with Couette geometry. The values in the MLV phase are in agreement with the previous data¹⁰ from 10 to 40 s⁻¹. The MLV radius was calculated using the analysis proposed by Samuels.⁵⁰ The capillary number was calculated using eq 3, while Ca* was calculated using the viscosity in the MLV phase.

where the MLV radii follow the behavior of $R \propto \dot{\gamma}^{-0.6}$ that is very close to that in eq 1. In general, at the same surfactant concentration the MLV size of C₁₂E₅ at 40 wt % in D₂O is found to be larger than for MLVs of C₁₂E₄, which are in turn larger than those for C₁₀E₃.¹⁴ Changes in the structural transition between L_a and MLVs and the shape anisotropy of the vesicles can be correlated via a dimensionless group known as the capillary number (sometimes referred to as a Weber number if the applied stress is predominantly viscous). The capillary number is the ratio of the distorting viscous stress of the flowing matrix and the restoring force of interfacial tension

$$Ca = \frac{(\eta_m \dot{\gamma} R_{\text{MLV}})^2}{(\Gamma / 2R_{\text{MLV}})} = \frac{\eta_m \dot{\gamma}^2 R_{\text{MLV}}}{\Gamma} \quad (3)$$

where η_m is the matrix viscosity that in this case is the heavy water viscosity at 55 °C (~0.6 mPa s) and Γ is the interfacial tension. Taylor predicted the droplet deformation in a shear flow, as defined by the droplet aspect ratio, as a function of the viscosity ratio of the droplet phase to that of the matrix. This was extended by Bergenholz and Wagner to apply to MLV formation using the interfacial tension model of van der Linden and coworkers, who identified the effective interfacial tension of an MLV as the geometric mean of the bulk rigidity and compressibility moduli.^{37,38,51} This is estimated to be ~10⁻⁴ N/m in lyotropic systems.⁵² As noted in that work, however, the

strength of shear forces acting in this concentrated system is more accurately represented by using the actual shear viscosity η_s in the MLV phase, rather than the medium viscosity (water) to calculate the capillary number. This capillary number based on the actual shear viscosity is denoted as Ca^* and is also shown in Table 1.

The Ca numbers indicate that the shear-induced MLVs form at very low values, whereas the Ca^* values are on the order that is expected and anticipated given the observations of Zilman and Granek⁴¹ and Bergenholz and Wagner.³⁷ Thus, a critical stress comparable to the effective interfacial tension sets the size of the MLVs, and a critical amount of strain is necessary to form MLVs.

The mechanism of the La-to-MLVs transition has been proposed to involve an intermediate structure as multilamellar cylinders MLCs,^{12,15,28,37} possibly following a coherent stripe buckling of the lamellar phase.⁵³

3.2. Lamellar Orientation during MLV Formation by Flow-SANS. The lamellar-to-multilamellar vesicle transition was observed by flow-SANS from the newly available gap prospective, i.e., 1–2 plane. Figure 2 shows the 2D SANS patterns obtained during MLV formation at a shear rate of 10 s^{-1} on both relative (upper) and absolute (lower) color rendering scales.

In the following discussion, L_α will be used to indicate planar lamellae. The prominent Bragg peak at 30 s corresponds to a major population of bilayers with their normal parallel to the gradient direction which is denoted the c orientation.^{36,41} This is the first important result; i.e., the existence of the L_α in the c orientation is proven here by SANS experiments in the 1–2 plane, while previous measurements could detect only a minority population of bilayers with their normal parallel to the vorticity direction, i.e., a orientation, because they were performed using the radial beam configuration.^{8,12,13} However, experiments performed in the tangential configuration report the existence of a c orientation.^{12,40} The sequence of structure evolution evident in Figure 2 for 1–2 flow SANS corresponds to that observed in Figure 1 using flow-SALS, where a transition occurs and saturates qualitatively after 450 s. Importantly, the sequence of structural evolutions in Figure 2 was observed to be the same for both forward and reverse shear directions (Supporting Information, Figure S2), where the 2D patterns are rotated 90° upon reversal of the direction of flow. $I(q)$ versus q plots for sector averages show that the lamellar structure is maintained during shear flow (Figure S3 in the Supporting Information). This confirms that the tilting of the lamellar phase is due to the shear flow.

Figure 3 shows the time evolution of azimuthal or angular variation of the diffracted SANS intensity within a sector mask of 360° in the q range between 0.07 and 0.09 \AA^{-1} . The GRASP output references the angle of 0° to be the positive vertical direction in the SANS patterns, which corresponds to the (negative) flow direction. The azimuthal trace changes from the c orientation (evident as sharp peaks centered around 90 and 270°) toward a broader, tilted pattern with broad peaks centered at ~65 and ~245° over a transition of about 800 s, and then no further changes are observed. There is also an increase in the SANS intensity evident at 9 ± 1 and $189 \pm 1^\circ$ upon reduction in the c -orientation peaks that is quantitatively reported in Figure 6. As these scattering intensity peaks correspond to the normal of the lamellae, this broadening and reorientation of the scattering intensity in the azimuthal angle indicates a reorganization of the c -oriented lamellar structure,

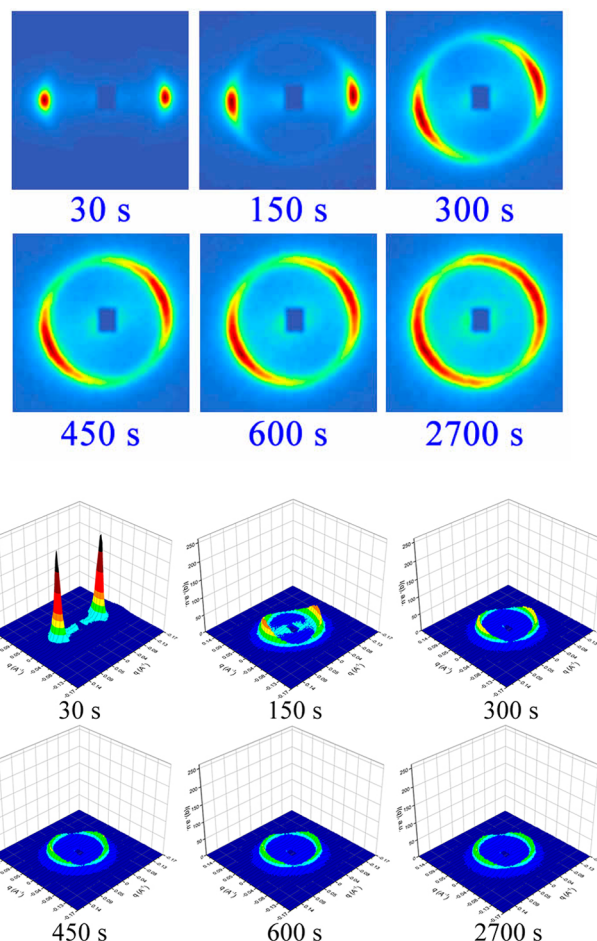


Figure 2. (Upper) Two-dimensional scattering patterns in the velocity-gradient plane as a function of time at a constant shear rate of 10 s^{-1} and a temperature of 55 °C for 40 wt % C₁₂E₅ in D₂O. The rotational direction of the shear cell environment is clockwise such that the shear direction is downward and the gradient direction is to the right in the laboratory frame of reference. The color scale is rescaled for each condition. (Lower) Topographical representation of the same data but on an absolute color scale.

which is highly ordered, into a much broader distribution of orientations with a primary axis tipped relative to the flow direction.

The tilt in the primary axis of the Bragg scattering arising from lamellar orientation under flow becomes constant by around 450 s. The angular position of the primary axis in Figure 4 was determined by following the intensity maxima in the azimuthal trace of the 2D patterns as a function of time. To better relate the real-space structure to the laboratory coordinate frame defined by the flow field, in the rest of this article the angle of this principle axis of scattering intensity will be referenced to the shear gradient direction for clockwise rotation, as shown in the inset of Figure 4.⁵⁴ This is a 90° rotation of the definition of the angle as defined in GRASP, which internally references the azimuthal angle to the vertical direction on the SANS patterns (Figure 3). As this Bragg scattering peak corresponds to the normal vector of the lamellar sheets, this angle also represents the orientation of the lamellar sheets themselves relative to the shear flow, where zero angle indicates flow alignment of the sheets along the flow direction and a positive angle below 90° represents lamellar sheets organized about a vector lying in the extensional quadrant of

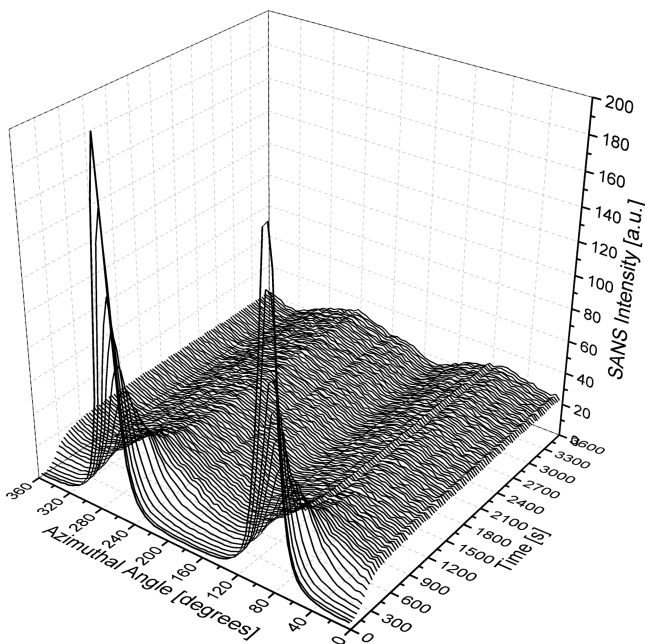


Figure 3. Time evolution of the azimuthal traces for 40 wt % $C_{12}E_5$ in D_2O at a shear rate of 10 s^{-1} and $55\text{ }^\circ\text{C}$. The azimuthal traces were extracted from sector masks of 360° in the q range between 0.07 and 0.09 \AA^{-1} . Note that the zero azimuthal angle is aligned along the flow direction.

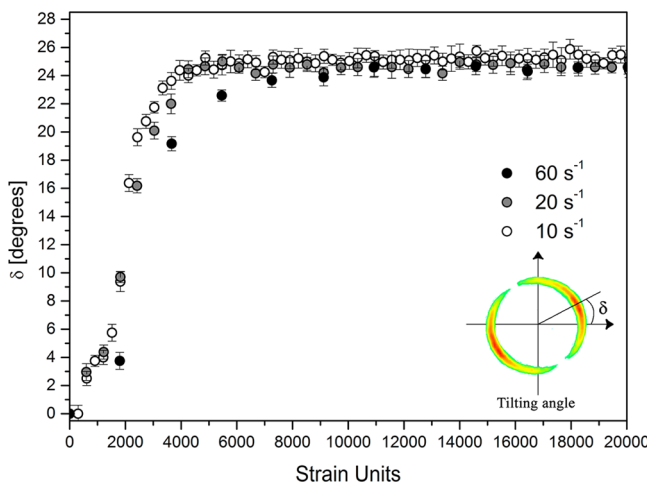


Figure 4. Strain dependence of the angular position of the Bragg peak for 10, 20, and 60 s^{-1} versus applied strain. Each experiment started from a nearly perfect c orientation and was performed at $55\text{ }^\circ\text{C}$. The inset shows the reference frame for defining the principle axis of the scattering relative to the flow gradient direction. In this new frame system, the angular position of the Bragg peak of c orientation of planar lamellae is 0° .

the flow. Angles between 90 and 180° correspond to the compressional quadrant of the flow, where much lower intensities are observed.

As seen in Figures 2 and 4, upon flow start up the peak tilting first increases away from flow alignment and then the pattern becomes significantly broader. Layer tilting, due to defect motion, has in fact been proposed to occur by Lu et al.^{55,56} In their model, they also predict a structural (undulation) instability when the tilt angle exceeds a critical value. Tilting of the layers starts immediately after the onset of flow (Figure

4). As can be seen in Figure 3, the decrease in the Bragg spot intensity also begins immediately after the onset of flow. Hence, simultaneously to the tilting, the layers are bent perpendicular to the velocity direction, which eventually leads to the cylindrically symmetric intermediate structure, presumably MLC, at ca. $\gamma = 3000$ as confirmed by other methods.^{12,28,29}

Note that a perfectly spherical MLC would produce a circular ring of constant intensity. Importantly, here, even at steady state the 2D SANS pattern is very broadly distributed in angle but is never fully isotropic under flow. In the following discussion, we refer only to the lowest of the two values of the alignment angle of the Bragg peak where the other is trivially related by symmetry. The center of the peak intensity distribution progresses from 0° to a final angle of $\delta = 25 \pm 1^\circ$ at steady state for all three shear rates examined (10 , 20 , and 60 s^{-1}). Note that the L_α -to-MLC transition, as shown by the complementary rheo-SALS measurements, is achieved when this alignment angle δ becomes constant. This indicates that the final tilting angle is not dependent on the applied shear rate, whereas during the transition to reach this steady state the δ angles approximately follow the applied strain. These results can be explained by considering that the anisotropy of the steady-state pattern is related to distorted MLVs under shear flow, while the changes in the tilting angle, before the steady state, are related to the inclination of the planar lamellae in the Couette gap. Figure 4 also shows that the transition in the δ angle is strain-controlled in agreement with previous observations.³⁷

To further verify the presence of stable MLVs, a sequence of start-stop experiments were performed from the oriented lamellar state at 10 s^{-1} . In Figure 5, the 2D SANS patterns recorded during steady shear and flow cessation are shown for each step.

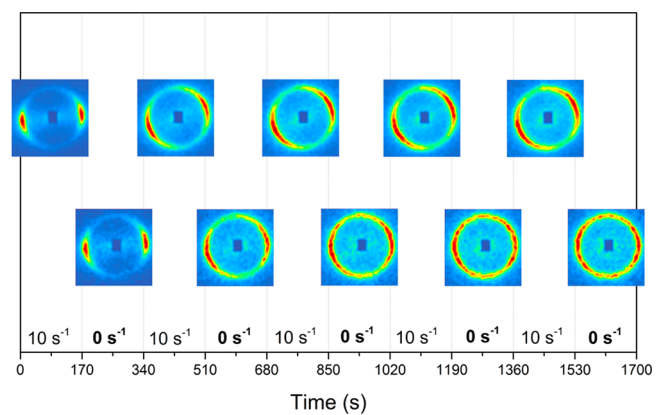


Figure 5. Start-stop experiment for 40 wt % $C_{12}E_5$ in D_2O at $55\text{ }^\circ\text{C}$. A constant shear rate of 10 s^{-1} is applied and interrupted every 170 s .

The reorganization of the MLVs into a lamellar phase is known to proceed by a very slow relaxation process, hence 170 s is sufficiently short to avoid the reverse transition. Under these experimental conditions, MLV formation is observed to be a continual process under flow that can be restarted from the point of flow cessation. When the shear flow is stopped, an isotropic SANS pattern is observed after 1300 s , i.e., after $\sim 800\text{ s}$ of the applied shear flow. The relaxation experiment reveals that (a) when the shear rate is stopped before the MLVs fully form, domains of tilted planar lamellae are entrapped in the overall c orientation of the lamellar phase and their relaxation

process is slow and (b) when the shear rate is stopped after MLV formation, the relaxation process is faster because the stretched but closed lamellar sheets in MLVs relax by an effective interfacial tension that drives the formation of an isotropic MLV shape at equilibrium.

3.3. Shear Rate Dependence. The L_α -to-MLV transition follows a similar pathway for the different shear rates probed. In Figure 6, the SANS intensities of boxes centered at 99 ± 1 and $279 \pm 1^\circ$ over the q range of $0.07\text{--}0.09 \text{\AA}^{-1}$ were averaged (tilted-flow direction, blue) at 0 and 180° (gradient direction, green) and 25 ± 1 and $205 \pm 1^\circ$ (tilted-gradient direction, red) at 10 , 20 , and 60 s^{-1} . Black open circles are the shear stress values.

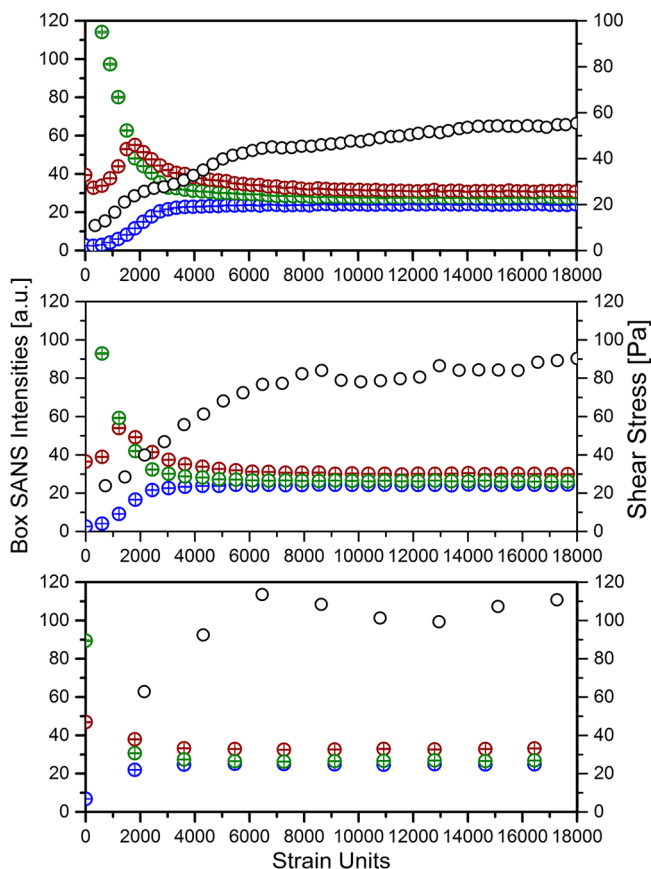


Figure 6. SANS and rheological data are plotted against strain units for 10 , 20 , and 60 s^{-1} from top to bottom, respectively. SANS intensities of boxes centered at 99 ± 1 and $279 \pm 1^\circ$ over the q range of $0.07\text{--}0.09 \text{\AA}^{-1}$ were averaged (tilted-flow direction, blue) at 0 and 180° (gradient direction, green) and 25 ± 1 and $205 \pm 1^\circ$ (tilted-gradient direction, red) at 10 , 20 , and 60 s^{-1} . Black open circles are the shear stress values.

$279 \pm 1^\circ$ (e.g., 9 ± 1 and $189 \pm 1^\circ$ in Figure 3) were averaged (tilted-flow direction, blue). The same procedure was followed for the boxes at 0 and 90° (gradient direction, green) and 25 ± 1 and $205 \pm 1^\circ$ at 10 , 20 , and 60 s^{-1} (tilted-gradient direction, red). Interestingly, for the intensity in the tilted gradient direction (red) a maximum appears between 1200 and 2000 strain units, which is commensurate with the presence of the MLC structure in rheo-SALS (Figure 1). Moreover, after 4500 strain units the intensity-time profiles start to become similar in all three directions, which is indicative of MLV formation. After ca. 8000 strain units for all shear rates, the transition reaches a final state and the MLVs are fully formed. Further small changes in the shear stress reflect the refinement of the structure. Importantly, changes in the relative intensities in these three directions are evident as transitions in the evolution of the shear stress, showing directly that the rheological

behavior reflects the reorganization of the lamellar structure into MLVs.

These new results now provide important evidence concerning the mechanism of MLV formation from the L_α phase. The results from this new point of view in the $1\text{--}2$ plane are consistent with a shear-induced buckling instability of the lamellar structure, as envisioned and predicted by Zilman and Granek.⁴¹ Namely, the lamellae undergo a highly anisotropic mechanical deformation during the strains leading to MLV formation that is consistent with lamellar buckling. Such buckling is pictured to be highly anisotropic (although the linear stability analysis leading to the instability is assumed to be Gaussian and therefore symmetric in the flow direction), and this drives the “rolling up” of the lamellar into closed structures. The unique and novel data presented here in the $1\text{--}2$ plane is crucial to determining the anisotropy associated with buckling; however, hints of this anisotropy are evident in prior works in the $1\text{--}3$ and $2\text{--}3$ planes of flow.^{37,57} Combining observations in all three planes of flow indicates that the instability appears in the $1\text{--}2$ plane of flow but must be fully three-dimensional to lead to the closed, onionlike structures observed in the steady state. In these prior works, the near isotropy of the SANS scattering was taken as a signature of MLV formation in contrast to the oriented Bragg peaks observed for the oriented L_α phases. However, those patterns show some weak anisotropy, which is shown here to be very rich when observed in the plane of flow.

Figure 7, which is based on the original sequence of Nettlesheim et al.¹² but now includes the important results obtained with the new instrumentation, summarizes the structural evolution leading to MLV formation. The data shown include complementary results for the $1\text{--}3^{10}$ plane and correspond to a shear rate of 10 s^{-1} . The transition can be subdivided into five steps. First (I) is the initial state of planar lamellae in the c orientation after the previously described alignment procedure. This is immediately followed by (II) the tilting of the lamellae due to the applied flow, which has now been more clearly differentiated by using time-resolved SANS experiments with the $1\text{--}2$ shear cell environment. These tilted and bended lamellae become unstable in three dimensions, and defects are generated, which leads to a temporary state consisting of a mixture of undulating and disorganized lamellae and some partially closed structures, such as MLCs (III). The presence of MLCs has been inferred from a large anisotropy evident in three-dimensional diffusion NMR experiments, where the water diffusion coefficient is observed to be large in the velocity direction relative to the other directions during MLV formation for the $C_{10}E_3/D_2O$ system.²⁹ The third step is the creation of closed lamellar sheets as proto-MLVs by the nonlinear growth of this shear-induced instability.^{12,28} Note that the maximum evident in the intensity measured in the neutral direction via the $1\text{--}3$ plane of observation occurs after the maximum observed at 25° in the $1\text{--}2$ plane. These observations are consistent with a mechanism whereby the lamellae first roll up in the plane of shear, forming tilted structures. This is accompanied by some orientation of lamella with normal vectors along the vorticity direction, which is indicative of MLCs and MLVs. Note that the angle of the principle axis of the scattering reaches nearly its final value at about the same strain as when the scattering intensity in the vorticity direction reaches a maximum. The flow instability is now highly nonlinear and fully three-dimensional. Upon further shear strain, the MLVs are refined (IV) toward a more spherical

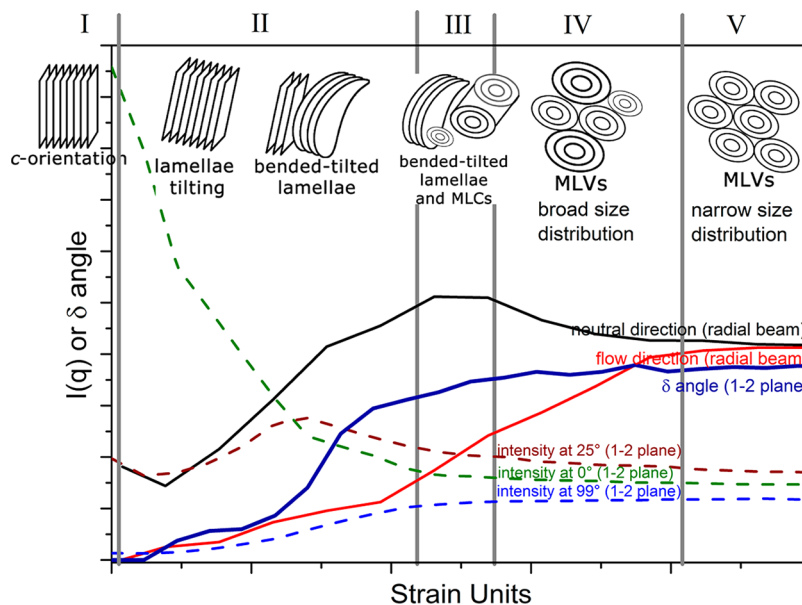


Figure 7. Outline of the process, showing the initial state of the lamellar phase, the tilting of the lamellae, the coherent stripe buckling or MLCs, a region where buckled lamellae and MLVs coexist, the state where MLVs are polydisperse, and the final state where MLVs are monodisperse. The intensity evolution in the radial (neutral direction, solid black line; flow, solid red line) and the intensities of the Bragg peak on the 1–2 plane (0° , dashed green line; 25° , dashed red line; 99° , dashed blue line) are shown together. Moreover, the tilt in the angle position of the Bragg peak is reported (solid blue line).

shape and well-defined size (as evident in the rheo-SALS). For the applied shear rate used for this illustration, a pure MLV state is reached (V). In the previous pioneering work,¹² such a mechanistic description of MLV formation was not possible. Here, the tilting of the lamellar phase at the beginning of the transition and the distortion of the MLVs at the end are obtained through the use of the new gap prospective sample environment.

To date, there is no theory capable of predicting the highly anisotropic structure of the buckled lamellar phase of surfactant solutions as this is a highly nonlinear state, but the robustness of the angle observed in our work suggests that a theory for this should be applicable to a broad range of MLV-forming systems. The data to test this future theory is presented here. However, the net lamellar alignment of the MLVs so formed may be simply related to the balance of interfacial tension and the applied shear stresses. On the basis of the success of the calculated value of Ca^* to relate the applied stress to the size of the MLVs formed, a similar model based on the concept of an effective interfacial tension may suffice to rationalize the net orientation angle of the lamellae in the MLVs under steady flow. Similar angular orientations have been measured for emulsions under shear flow.⁵⁸ Fonseca and Herrmann studied the settling velocity and the average orientation of the ellipsoids as a function of volume fraction that show a local maximum which disappears as the Reynolds number is increased. Cell models for emulsion rheology are capable of capturing the relationship among the applied shear flow, surface tension, droplet size, concentration, and rheological properties of the phases,^{59,60} and may prove relevant for understanding the novel observations reported here for MLV shear orientation.

3.4. Comparison with $C_{10}E_3$. The complementary $C_{10}E_3/D_2O$ system was investigated in order to further illustrate the robustness of our new observations concerning the pathway of the intensity distribution during the L_α -to-MLV transition. A similar behavior is observed, so only the angular position of the

intensity maximum is presented, as calculated and referenced for the $C_{12}E_5$ system. The angle position of the intensity maximum shown in Figure 8 shows the same behavior as for

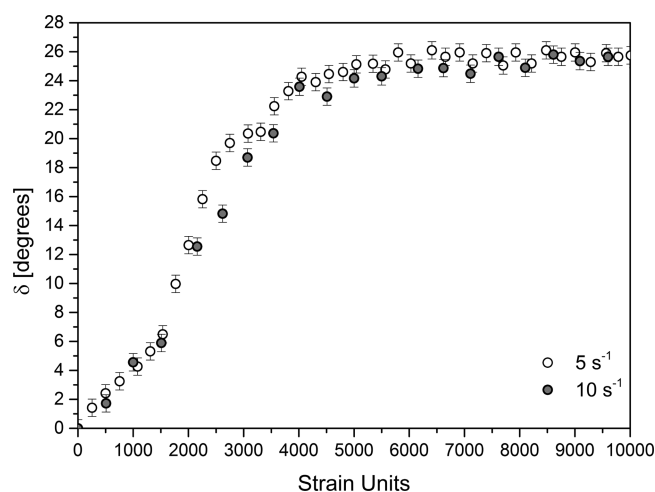


Figure 8. Strain dependence of the angular position of the Bragg peak for $5\text{ }^\circ\text{C}$ and 10 s^{-1} ($40\text{ }^\circ\text{C}$). The system investigated is 40 wt % $C_{10}E_3$ in D_2O .

the $C_{12}E_5$ system. The peak tilting increases, and the pattern changes from anisotropic to less anisotropic. The intensity distribution center moves from 0° to an angle of $\delta = 25 \pm 1^\circ$ in the steady state for shear rates of 5 s^{-1} at $25\text{ }^\circ\text{C}$ and 10 s^{-1} at $40\text{ }^\circ\text{C}$. Thus, for the L_α -to-MLV transition the steady state of the δ angle position is the same for two systems. Figure 3 also shows that the MLV formation as evinced by the saturation of the δ angle reaches steady state at a comparable number of strain units as for $C_{12}E_5/D_2O$. Furthermore, the Ca^* number calculated using literature data for the viscosity and MLV size¹² is 4.7 for both shear rates of 5 and 10 s^{-1} ($25\text{ }^\circ\text{C}$);

however, when other literature data are used, the Ca^* number is found to be 3.4 for 10 s^{-1} . Unfortunately, no MLV size data are available at $40\text{ }^\circ\text{C}$. However, these Ca^* numbers are consistent with the previous result in Table 1 for the C_{12}E_5 system; in fact, at 10 s^{-1} a Ca^* number of around 4 is common for both systems. In the case of C_{12}E_4 ,³⁹ the Ca^* numbers at $25\text{ }^\circ\text{C}$ for 5 and 10 s^{-1} are 2.9 and 4.5, respectively. For comparison, using the data of Suganuma et al.¹⁶ obtained by rheo-SALS equipped with a Couette yields Ca^* values of 1.9 and 2.0, respectively. These results show that when considered as a function of strain and capillary number, these two MLV-forming systems show remarkably consistent behavior and the same buckling-formation mechanism.

3.5. Temperature and Shear Rate Effect. The relative stability of MLVs and planar lamellae was mapped as a function of temperature (spontaneous curvature) and shear rate, as shown in Figure 9. Two-dimensional SANS patterns obtained

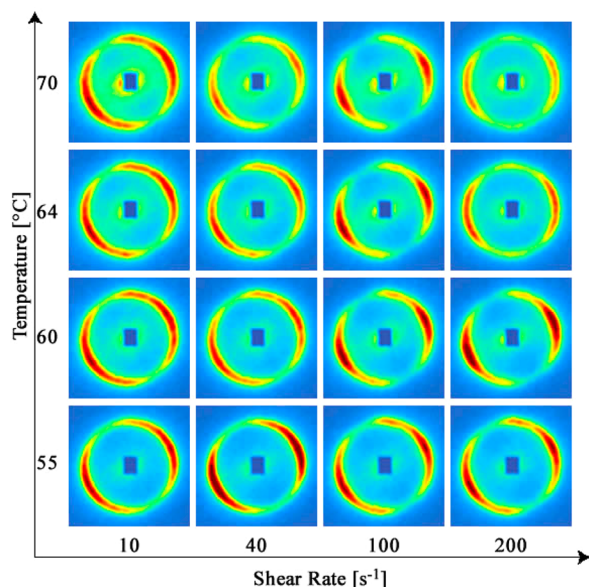


Figure 9. Steady-state scattering patterns as a function of temperature and shear rate for 40 wt % C_{12}E_5 in D_2O .

in the 1–2 plane, i.e., from the Couette gap, for 40 wt % C_{12}E_5 in D_2O were reported. As observed, the angular position of the intensity maximum is nearly constant. However, at high shear rates, Bragg peaks along the flow direction are evident, consistent with small amounts of *b*-oriented L_α . These can be associated with MLV structures. However, the temperature has an effect that is particularly evident at 200 s^{-1} .

The anisotropic 2D SANS patterns are due to distorted MLVs. MLVs are formed at low shear rate, whereas at higher temperatures and high shear rates the MLV phase competes with the L_α . Note that the *a*-oriented L_α phase has a Bragg vector along the incident beam direction, so it is not visible in the novel 1–2 plane geometry (but was evident in the SALS patterns in the 1–3 plane). In fact, at 200 s^{-1} between 64 and $70\text{ }^\circ\text{C}$ the SANS patterns can be largely attributed to L_α . The tilting angle seems to be affected by high shear rates and temperature such that further investigations are needed to quantitatively evaluate the tilting angle's dependence on concentration, temperature, and shear rate. This last result is in agreement with a previous study on C_{12}E_5 ,¹⁰ where the

relative stability of the MLVs was reported. This shear melting is also evident in the SALS data reported in Figure 1.

4. CONCLUSIONS

Novel measurements of MLV formation in the 1–2 plane of flow by SANS using a new sample environment available at the ILL Grenoble and NCNR NIST show the time evolution of MLVs forming from the shear-oriented L_α phase. The patterns recorded in the flow shear gradient plane are due to the major population of bilayers, i.e., *c* orientation. By following the transition from the Couette gap, a tilt in the angular position of the Bragg peak was observed due to the applied shear rate. The tilt is also present after the formation of the MLVs; however, the anisotropy is much less sharp than in the L_α phase, and the anisotropy in the patterns indicates a shear-induced deformation of MLVs, qualitatively similar to what is observed in flowing emulsions. This structural evolution is consistent with lamellar planes oriented in the extensional quadrant of the flow as anticipated for nonlinear buckling. A nonlinear buckling instability in the plane of shear is followed by an instability in the vorticity direction that generates a full three-dimensional instability of the lamellar phase generating MLVs. The size of the MLVs was obtained by rheo-small angle light scattering, and the combined methods demonstrated that a critical capillary number defines the state of the stable MLV phase. Furthermore, the evolution of the lamellar tilt angle during MLV formation follows the strain for all applied shear rates. The primary axis of lamellar orientation in the MLV state was found to be constant under flow at $25\text{ }^\circ\text{C}$ relative to the flow gradient direction, indicating a preferred orientation of the lamellae comprising the MLVs in a direction in the extensional quadrant of the shear flow. These results are shown to be quantitatively robust for a similar nonionic surfactant system of lower chain length and for a wide variation in temperature, suggesting these new and novel observations may be representative of MLV formation more broadly. The quantitative data provided here is a basis for theoretical models that seek to describe this scientifically intriguing and technologically useful nonequilibrium microstructural transition.

ASSOCIATED CONTENT

S Supporting Information

Schematic diagram of the flow-SANS setup. Tilted 2D patterns recorded in the 1–2 plane under shear flow during multilamellar vesicle formation. SANS intensity along sector averages ± 5 oriented along the principle axis of the scattering intensity. This material is available free of charge via the Internet at <http://pubs.acs.org>.

AUTHOR INFORMATION

Notes

The authors declare no competing financial interest.

ACKNOWLEDGMENTS

The beam line was provided by the Institut-Laue-Langevin under proposal 57735 and by the NCNR NIST under proposal S29-25. We acknowledge the support of the National Institute of Standards and Technology, U.S. Department of Commerce, in providing the neutron research facilities used in this work. This work utilized facilities supported in part by the National Science Foundation under agreement no. DMR-0944772. This

article was prepared in part (N.J.W.) under cooperative agreements 70NANB10H256 and 70NANB12H239 from NIST, U.S. Department of Commerce. The statements, findings, conclusions, and recommendations are those of the author(s) and do not necessarily reflect the view of NIST or the U.S. Department of Commerce. This article was also cofinanced by the European Commission, European Social Fund, and the Region of Calabria. The authors are solely responsible for this article, and the European Commission and the Region of Calabria are not responsible for any use that may be made of the information contained herein. We acknowledge financial support from the European Commission under the Seventh Framework Program by means of the grant agreement for the Integrated Infrastructure Initiative no. 262348 European Soft Matter Infrastructure (ESMI).

■ REFERENCES

- (1) Holmberg, K.; Jönsson, B.; Kronberg, B.; Lindman, B. *Surfactants and Polymers in Aqueous Solution*; John Wiley & Sons: Chichester, West Sussex, England, 2003.
- (2) Cuomo, F.; Lopez, F.; Angelico, R.; Colafemmina, G.; Ceglie, A. Nucleotides and nucleolipids derivatives interaction effects during multi-lamellar vesicles formation. *Colloids Surf., B* **2008**, *64*, 184–193.
- (3) Oswald, P.; Ben-Abraham, S. I. Undulation instability under shear in smectic A liquid crystals. *J. Phys. (Paris)* **1982**, *43*, 1193–1197.
- (4) Oswald, P.; Kléman, M. Lubrication theory of smectic A phases. *J. Phys. Lett.* **1982**, *43*, 411–415.
- (5) Diat, O.; Roux, D. Preparation of monodisperse multilayer vesicles of controlled size and high encapsulation ratio. *J. Phys. II France* **1993**, *3*, 9–14.
- (6) Roux, D.; Nallet, F.; Diat, O. Rheology of Lyotropic Lamellar Phases. *Europhys. Lett.* **1993**, *24*, 53–58.
- (7) Diat, O.; Roux, D.; Nallet, F. Effect of Shear on a Lyotropic Lamellar Phase. *J. Phys. II* **1993**, *3*, 1427–1452.
- (8) Le, T. D.; Olsson, U.; Mortensen, K.; Zipfel, J.; Richtering, W. Nonionic amphiphilic bilayer structures under shear. *Langmuir* **2001**, *17*, 999–1008.
- (9) Gentile, L.; F.B. Silva, B.; Balog, S.; Mortensen, K.; Olsson, U. Structural transitions induced by shear flow and temperature variation in a nonionic surfactant/water system. *J. Colloid Interface Sci.* **2012**, *372*, 32–39.
- (10) Gentile, L.; Oliviero Rossi, C.; Olsson, U.; Ranieri, G. A. Effect of Shear Rates on the MLV Formation and MLV Stability Region in the C₁₂E₅/D₂O System: Rheology and Rheo-NMR and Rheo-SANS Experiments. *Langmuir* **2011**, *27*, 2088–2092.
- (11) Gentile, L.; Silva, B. F. B.; Lages, S.; Mortensen, K.; Kohlbrecher, J.; Olsson, U. Rheochoas and flow instability phenomena in a nonionic lamellar phase. *Soft Matter* **2013**, *9*, 1133–1140.
- (12) Nettesheim, F.; Zipfel, J.; Olsson, U.; Renth, F.; Lindner, P.; Richtering, W. Pathway of the Shear-Induced Transition between Planar Lamellae and Multilamellar Vesicles as Studied by Time-Resolved Scattering Techniques. *Langmuir* **2003**, *19*, 3603–3618.
- (13) Le, T. D.; Olsson, U.; Mortensen, K. Packing states of multilamellar vesicles in a nonionic surfactant system. *Phys. Chem. Chem. Phys.* **2001**, *3*, 1310–1316.
- (14) Medronho, B.; Shafaei, S.; Szopko, R.; Miguel, M. G.; Olsson, U.; Schmidt, C. Shear-induced transitions between a planar lamellar phase and multilamellar vesicles: continuous versus discontinuous transformation. *Langmuir* **2008**, *24*, 6480–6486.
- (15) Medronho, B.; Brown, J.; Graça Miguel, M.; Schmidt, C.; Olsson, U.; Galvosas, P. Planar lamellae and onions: a spatially resolved rheo-NMR approach to the shear-induced structural transformations in a surfactant model system. *Soft Matter* **2011**, *7*, 4938–4947.
- (16) Suganuma, Y.; Imai, M.; Kato, T.; Olsson, U.; Takahashi, T. Order–Disorder Transition of Nonionic Onions under Shear Flow. *Langmuir* **2010**, *26*, 7988–7995.
- (17) Ito, M.; Kosaka, Y.; Kawabata, Y.; Kato, T. Transition Processes from the Lamellar to the Onion State with Increasing Temperature under Shear Flow in a Nonionic Surfactant/Water System Studied by Rheo-SAXS. *Langmuir* **2011**, *27*, 7400–7409.
- (18) Zipfel, J.; Lindner, P.; Richtering, W. Shear induced order and disorder in lyotropic lamellar phases. *Prog. Colloid Polym. Sci.* **1998**, *110*, 139–143.
- (19) Zipfel, J.; Berghausen, J.; Lindner, P.; Richtering, W. Influence of Shear on Lyotropic Lamellar Phases with Different Membrane Defects. *J. Phys. Chem. B* **1999**, *103*, 2841–2849.
- (20) Penfold, J.; Staples, E.; Khan Lodhi, A.; Tucker, I.; Tiddy, G. J. T. Shear-Induced Transformations in the Lamellar Phase of Hexaethylene Glycol Monohexadecyl Ether. *J. Phys. Chem. B* **1997**, *101*, 66–72.
- (21) Åslund, I.; Medronho, B.; Topgaard, D.; Söderman, O.; Schmidt, C. Homogeneous length scale of shear-induced multilamellar vesicles studied by diffusion NMR. *J. Magn. Reson.* **2011**, *209*, 291–299.
- (22) Sato, D.; Obara, K.; Kawabata, Y.; Iwahashi, M.; Kato, T. Re-entrant Lamellar/Onion Transition with Varying Temperature under Shear Flow. *Langmuir* **2013**, *29*, 121–132.
- (23) van der Linden, E.; Hogervorst, W. T.; Lekkerkerker, H. N. W. Relation between the Size of Lamellar Droplets in Onion Phases and Their Effective Surface Tension. *Langmuir* **1996**, *12*, 3127–3130.
- (24) Panizza, P.; Roux, D.; Vuillaume, V.; Lu, C.-Y. D.; Cates, M. E. Viscoelasticity of the Onion Phase. *Langmuir* **1996**, *12*, 248–252.
- (25) Berghausen, J.; Zipfel, J.; Lindner, P.; Richtering, W. Shear-induced orientations in a lyotropic defective lamellar phase. *Europhys. Lett.* **1998**, *43*, 683.
- (26) Fujii, S.; Richtering, W. Shear quench-induced disintegration of a nonionic surfactant C10E3 onion phase. *Soft Matter* **2013**, *9*, 5391–5400.
- (27) Butler, P. Shear induced structures and transformations in complex fluids. *Curr. Opin. Colloid Interface Sci.* **1999**, *4*, 214–221.
- (28) Zipfel, J.; Nettesheim, F.; Lindner, P.; Le, T. D.; Olsson, U.; Richtering, W. Cylindrical intermediates in a shear-induced lamellar-to-vesicle transition. *Europhys. Lett.* **2001**, *53*, 335–341.
- (29) Medronho, B.; Olsson, U.; Schmidt, C.; Galvosas, P. Transient and Steady-State Shear Banding in a Lamellar Phase as Studied by Rheo-NMR. *Z. Phys. Chem.* **2012**, *226*, 1293–1313.
- (30) Gentile, L.; Behrens, M. A.; Balog, S.; Mortensen, K.; Ranieri, G. A.; Olsson, U. Dynamic Phase Diagram of a Nonionic Surfactant Lamellar Phase. *J. Phys. Chem. B* **2014**, *118*, 3622–3629.
- (31) Bergmeier, M.; Gradielski, M.; Hoffmann, H.; Mortensen, K. Behavior of ionically charged lamellar systems under the influence of a shear field. *J. Phys. Chem. B* **1999**, *103*, 1605–1617.
- (32) Koschoreck, S.; Fujii, S.; Lindner, P.; Richtering, W. Multilamellar vesicles (“onions”) under shear quench: pathway of discontinuous size growth. *Rheol. Acta* **2009**, *48*, 231–240.
- (33) Zipfel, J.; Berghausen, J.; Schmidt, G.; Lindner, P.; Alexandridis, P.; Tsianou, M.; Richtering, W. Shear induced structures in lamellar phases of amphiphilic block copolymers. *Phys. Chem. Chem. Phys.* **1999**, *1*, 3905–3910.
- (34) Pommella, A.; Caserta, S.; Guida, V.; Guido, S. Shear-Induced Deformation of Surfactant Multilamellar Vesicles. *Phys. Rev. Lett.* **2012**, *108*, 138301.
- (35) Safinya, C. R.; Sirota, E. B.; Plano, R. J. Nematic to smectic-A phase transition under shear flow: A nonequilibrium synchrotron x-ray study. *Phys. Rev. Lett.* **1986**, *66*, 068103.
- (36) Safinya, C. R.; Sirota, E. B.; Bruinsma, R. F.; Jeppesen, C.; Plano, R. J.; Wenzel, L. J. Structure of membrane surfactant and liquid crystalline smectic lamellar phases under flow. *Science* **1993**, *261*, 588–591.
- (37) Bergenholz, J.; Wagner, N. J. Formation of AOT/brine multilamellar vesicles. *Langmuir* **1996**, *12*, 3122–3126.
- (38) Vanderlinde, E.; Droege, J. H. M. Deformability of Lamellar Droplets. *Physica A* **1993**, *193*, 439–447.

- (39) Müller, S.; Börschig, C.; Gronski, W.; Schmidt, C.; Roux, D. Shear-Induced States of Orientation of the Lamellar Phase of C₁₂E₄/Water. *Langmuir* **1999**, *15*, 7558–7564.
- (40) Dhez, O.; Nallet, F.; Diat, O. Influence of screw dislocations on the orientation of a sheared lamellar phase. *Europhys. Lett.* **2001**, *55*, 821.
- (41) Zilman, A. G.; Granek, R. Undulation instability of lamellar phases under shear: A mechanism for onion formation? *Eur. Phys. J. B* **1999**, *11*, 593–608.
- (42) Courbin, L.; Delville, J. P.; Rouch, J.; Panizza, P. Instability of a lamellar phase under shear flow: formation of multilamellar vesicles. *Phys. Rev. Lett.* **2002**, *89*, 148305.
- (43) Courbin, L.; Pons, P.; Rouch, J.; Panizza, P. How do closed-compact multi-lamellar droplets form under shear flow? A possible mechanism. *Europhys. Lett.* **2003**, *61*, 275.
- (44) Marlow, S. W.; Olmsted, P. D. The effect of shear flow on the Helfrich interaction in lyotropic lamellar systems. *Eur. Phys. J. E* **2002**, *8*, 485–497.
- (45) Gurnon, A. K.; Godfrin, P. D.; Wagner, N. J.; Eberle, A. P. R.; Butler, P.; Porcar, L. Measuring Material Microstructure under Flow Using 1-2 plane flow-Small Angle Neutron Scattering. *J. Visualized Exp.* **2014**, *84*, e51068.
- (46) Liberatore, M. W.; Nettesheim, F.; Wagner, N. J. Spatially resolved small-angle neutron scattering in the 1-2 plane: A study of shear-induced phase-separating wormlike micelles. *Phys. Rev. E* **2006**, *73*, 020504(R).
- (47) Strey, R.; Schomäcker, R.; Roux, D.; Nallet, F.; Olsson, U. Dilute lamellar and L3 phases in the binary water–C₁₂E₅ system. *J. Chem. Soc., Faraday Trans.* **1990**, *86*, 2253–2261.
- (48) Laue-Langevin, I. Large dynamic range small-angle diffractometer D22. <http://www.ill.eu/instruments-support/instruments-groups/instruments/d22/>.
- (49) Glinka, C. J.; Barker, J. G.; Hammouda, B.; Krueger, S.; Moyer, J. J.; Orts, W. J. The 30 m Small-Angle Neutron Scattering Instruments at the National Institute of Standards and Technology. *J. Appl. Crystallogr.* **1998**, *31*, 430–445.
- (50) Samuels, R. J. Small-angle light scattering from optically anisotropic spheres and disks. Theory and experimental verification. *J. Polym. Sci. Part A-2* **2003**, *9*, 2165–2246.
- (51) van der Linden, E.; Hogervorst, W. T.; Lekkerkerker, H. N. W. Relation between the size of lamellar droplets in onion phases and their effective surface tension. *Langmuir* **1996**, *12*, 3127–3130.
- (52) Petrov, A. G. *The Lyotropic State of Matter: Molecular Physics and Living Matter Physics*; CRC Press: Amsterdam, 1999.
- (53) Bruinsma, R.; Rabin, Y. Shear-Flow Enhancement and Suppression of Fluctuations in Smectic Liquid-Crystals. *Phys. Rev. A* **1992**, *45*, 994–1008.
- (54) Gurnon, A. K.; Godfrin, P. D.; Wagner, N. J.; Eberle, A. P. R.; Butler, P.; Porcar, L. Measuring Material Microstructure under Flow Using 1-2 plane flow-Small Angle Neutron Scattering. *Journal of Visual Experiments* **2014**, e51068.
- (55) Lu, C.-Y. D. Sizes of Multilamellar Vesicles in Shear. *Phys. Rev. Lett.* **2012**, *109*, 128304.
- (56) Lu, C.-Y. D.; Chen, P.; Ishii, Y.; Komura, S.; Kato, T. Non-linear rheology of lamellar liquid crystals. *Eur. Phys. J. E* **2008**, *25*, 91–101.
- (57) Zipfel, J.; Lindner, P.; Tsianou, M.; Alexandridis, P.; Richtering, W. Shear-induced formation of multilamellar vesicles (“onions”) in block copolymers. *Langmuir* **1999**, *15*, 2599–2602.
- (58) Fonseca, F.; Herrmann, H. J. Sedimentation of oblate ellipsoids at low and moderate Reynolds numbers. *Physica A* **2004**, *342*, 447–461.
- (59) Choi, S. J.; Schowalter, W. R. Rheological properties of nondilute suspensions of deformable particles. *Phys. Fluids* **1975**, *18*, 420–427.
- (60) Kernick, W. A., III; Wagner, N. J. The role of liquid-crystalline polymer rheology on the evolving morphology of immiscible blends containing liquid-crystalline polymers. *J. Rheol.* **1999**, *43*, 521–549.